

Visualization of convective boiling heat transfer in single microchannels with different shaped cross-sections

Tzu-Hsiang Yen ^{a,*}, Masahiro Shoji ^a, Fumio Takemura ^a,
Yuji Suzuki ^b, Nobuhide Kasagi ^b

^a *Energy Technology Research Institute, National Institute of Advanced Industrial Science and Technology (AIST),
1-2-1 Namiki, Tsukuba-shi, Ibaraki 305-8564, Japan*

^b *Department of Mechanical Engineering, The University of Tokyo, 7-3-1 Hongo, Bunkyo-ku, Tokyo 113-8656, Japan*

Received 4 August 2005

Available online 27 June 2006

Abstract

Convective boiling in transparent single microchannels with similar hydraulic diameters but different shaped cross-sections was visualized, along with simultaneous measurement of the local heat transfer coefficient. Two types of microchannels were tested: a circular Pyrex glass microtube (210 μm inner diameter) and a square Pyrex glass microchannel (214 μm hydraulic diameter). A 100-nm-thick semi-transparent ITO/Ag thin film sputtered on the outer wall of the microchannel was used for direct joule heating of the microchannel.

The flow field visualization showed semi-periodic variation in the flow patterns in both the square and circular microchannels. Such variation was because the confined space limited the bubble growth in the radial direction.

In the square microchannel, both the number of nucleation bubbles and the local heat transfer coefficient increased with decreasing vapor quality. The corners acted as active nucleation cavities, leading to the higher local heat transfer coefficient. In contrast, lack of cavities in the smooth glass circular microchannel yielded a relatively smaller heat transfer coefficient at lower vapor quality. Finally, the heat transfer coefficient was higher for the square microchannel because corners in the square microchannel acted as effective active nucleation sites.

© 2006 Elsevier Ltd. All rights reserved.

1. Introduction

Convective boiling and two-phase flow heat transfer characteristics in microchannels have become an important issue because they are dominant parameters in the performance of cooling systems for electronic devices, highly efficient compact heat exchangers [1], and reformers for methane direct micro fuel cells.

Convective boiling heat transfer characteristics in minichannels and microchannels have recently been extensively studied. For engineering applications, most of these studies focused on measuring the average heat transfer coefficient h in parallel microchannels; Ravigururajan [2] measured the

coefficient for parallel square microchannels (0.425 mm hydraulic diameter), and Steinke and Kandlikar [3] for SUS304 parallel microchannels (214 μm width, 200 μm depth and 57.15 mm length). Visualization experiments have revealed that flow patterns vary drastically due to the interactions between parallel microchannels. For example, Hetsroni et al. [4] visualized convective boiling in triangular parallel microchannels to study bubble growth dynamics, and found very unstable flow field and reverse flow, similar to the results by Steinke and Kandlikar [3]. Wu and Cheng [5] reported large variation in the flow field and periodic variations in the flow patterns in parallel microchannels.

These previous observations reveal that for detailed clarification of the heat transfer mechanism in microchannels, measurement of h in single microchannels with simultaneous visualization of the flow field is crucial to eliminate

* Corresponding author. Present address: Nissan Motor Co. Ltd., 560-2, Okatsukoku, Atsugi-shi, Kanagawa 243-0192, Japan.

E-mail address: thyen@mail.nissan.co.jp (T.-H. Yen).

Nomenclature

Bo	boiling number = $q/(h_{lv}\dot{m})$	P_{sat}	saturated pressure (Pa)
C_p	specific heat at constant pressure (J/(kg K))	Q	heat flux (W/m^2)
F	friction factor = $\Delta P_{sub}/(\frac{1}{2}\rho U^2 \frac{L}{D_i})$	$T_{w,out}$	outer wall temperature ($^{\circ}C$)
D_o	outer tube diameter (m)	$T_{w,in}$	inner wall temperature ($^{\circ}C$)
D_i	inner tube diameter (m)	t	relative time history of flow patterns (s)
h_{loss}	heat loss coefficient ($W/(m^2 K)$)	ΔP_{fl}	single phase pressure loss (Pa)
h_{lv}	latent heat (J/kg)	ΔP_{sub}	pressure loss of the subcooled liquid region (Pa)
h	heat transfer coefficient ($W/(m^2 K)$)	ΔP_{sup}	pressure loss of the superheated gas region (Pa)
I	electric current through the test section (A)	ΔP_{total}	total pressure loss in the test section (Pa)
k	thermal conductivity ($W/(m K)$)	ρ_l	liquid density (kg/m^3)
l	axial length of the subcooled liquid region (m)	ρ_v	vapor density (kg/m^3)
L	total length of the test section (m)	x	axial coordinate (m)
\dot{m}	mass flux ($kg/(m^2 s)$)	χ	vapor quality
P_{in}	pressure at the test section inlet (Pa)		

the effects of interactions between parallel microchannels. However, due to the high demand for measurement accuracy, experimental data for single microchannels is scarce. Saitoh et al. [6] measured the local h of single circular microtubes (1.12 and 0.51 mm ID) with R-134a refrigerant, and Yen et al. [7] measured it for single SUS 304 circular microtubes (0.19–0.51 mm ID). Their experimental results show that local heat transfer characteristics in single microchannels are qualitatively similar to those in parallel microchannels; namely, the local heat transfer coefficient decreases with increasing vapor quality and is relatively unaffected by heat flux and mass flux. Due to lack of experimental studies on convective boiling visualization in single microtubes, details of the physical mechanism and the importance of interactions between the channels still remain unclear.

Based on experimental results by Yen et al. [7], Steinke and Kandlikar [3], Yen et al. [7] and Kandlikar [8] concluded that bubble nucleation becomes the dominant mechanism in the heat transfer characteristics of microchannels. The relation between bubble nucleation and heat transfer characteristics must therefore be clarified in detail. Lee et al. [9] investigated the bubble growth dynamics in single microchannels as small as 41.3 μm ID, and concluded that a conventional bubble departure model for convective boiling in conventional tubes larger than 6 mm ID cannot predict the bubble growth and that the bubbles always nucleate from corners. Chung and Kawaji [10] investigated the effect of circular and square cross-sections in micro capillaries in adiabatic two-phase flow. They found that, although only slug and annular flows occurred in the micro capillaries, the flow maps for these flow patterns under different liquid and gas superficial velocities differed significantly between circular and square micro capillaries. Namely, the transition of flow patterns occurred at lower liquid and gas superficial velocity for the circular capillary than for the square capillary. Based on these previous observations, effect of cross-section

shape on the heat transfer characteristics in microchannels is critical because corners are dominant parameters in these heat transfer characteristics. Convective boiling experiments in microchannels smaller than 0.5 mm ID have not yet focused on the cross-section shape.

The purpose of this current study was to investigate effects of cross-section shape of microchannels on the heat transfer characteristics and to clarify the role of corners in square microchannels on bubble nucleation. This was accomplished by flow visualization experiments of convective boiling heat transfer in single microchannels that had square or circular cross-section with simultaneous measurement of local h .

2. Experimental setup

Fig. 1 shows a schematic of the flow loop used for the flow visualization and h measurement using HCFC123 as the working fluid. A twin plunge pump provided a mass flux \dot{m} from 100 to 800 $kg/m^2 s$. Unlike a single plunge pump, a twin plunge pump maintains a constant flow rate without introducing unwanted bubbles into the test section. The uncertainty interval in the flow rate was within $\pm 1\%$.

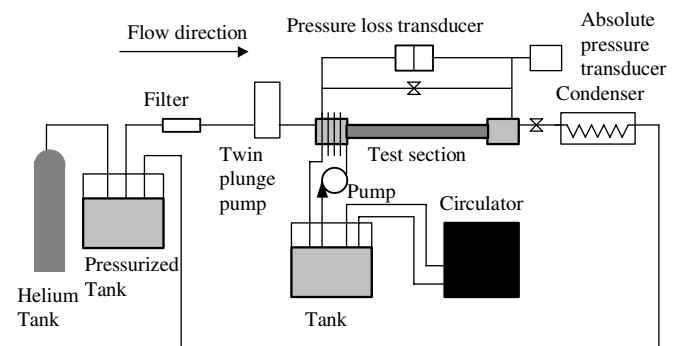


Fig. 1. Experimental loop.

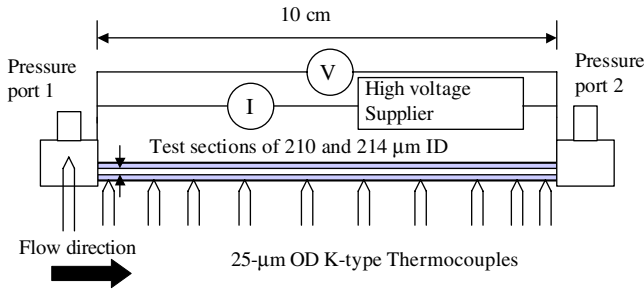
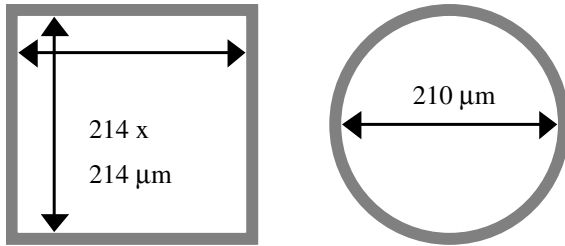
Fig. 2. Microchannel test section (210 or 214 μm).

Fig. 3. Cross-section shapes of microchannel test sections.

Fig. 2 shows a schematic of the test section. Two single microchannels made of Pyrex glass with different inner wall cross-sections were used as shown in Fig. 3. The circular cross-section was 0.21 mm ID and 0.4 mm OD, and the square cross-section was 0.214 mm in hydraulic diameter and 1.8 mm OD. Note that the outer wall of the square cross-section microchannel was circular and thus provided the ideal shape for estimation of heat loss.

To heat the microchannel, a thin film of Indium Tin Oxide (ITO) and silver was evenly sputtered to a thickness of about 100 nm on the outer surface of each microchannel. Fig. 4 shows a representative SEM photo of the sputtered thin film. The total resistance of the sputtered

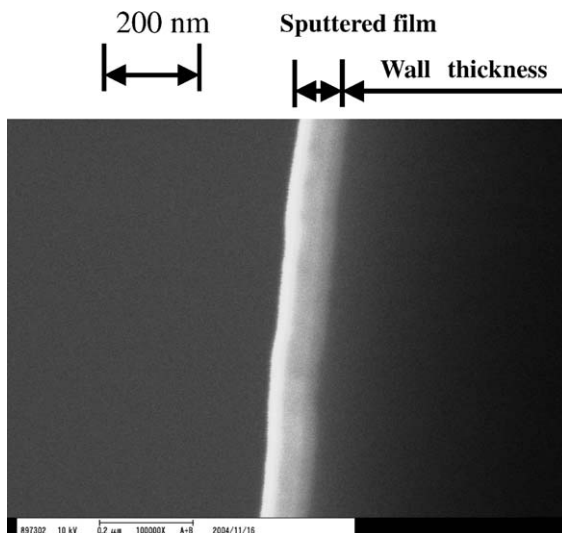


Fig. 4. Representative SEM photo of thin ITO/Ag film (100-nm thick) sputtered on the outer wall of the test section.

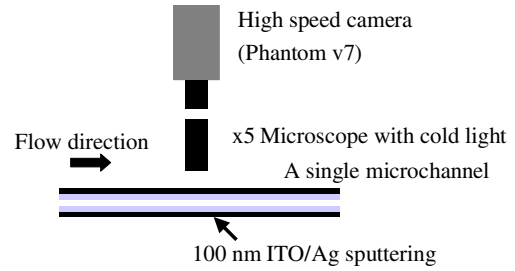


Fig. 5. Visualization setup.

microchannel was about 126 Ω for the square microchannel and 650 Ω for the circular microchannel. The outer wall temperature data of each microchannel were measured using nine *K*-type thermocouples (25- μm OD), which was calibrated within an accuracy of ± 0.1 K, glued to the outer surface of the microchannel using thermally conductive silicon.

A high-speed CMOS camera (Vision Research, Phantom v7) with a 5 \times microscope as the lens was used for the flow visualization inside the microchannels. Fig. 5 shows a schematic of the flow visualization apparatus. The images had a resolution of 700 \times 105 pixels and were taken at 24,000 frames/s.

3. Data reduction

The data reduction method used to obtain local heat transfer coefficient h and vapor quality, χ , was based on a similar method used by Yen et al. [7]. First, a preliminary heating experiment with an empty test section (i.e., no refrigerant) was done to estimate the heat loss h_{loss} to the air:

$$h_{\text{loss}} = \frac{q_{\text{loss}}}{(T_{\text{w,out}} - T_{\text{air}})}, \quad (1)$$

where $T_{\text{w,out}}$ is the outer wall temperature and T_{air} is the environment temperature. Then, heat flux q (W/m^2) can be calculated as

$$q = I^2 R / \pi D_i - q_{\text{loss}}, \quad (2)$$

where $I^2 R$ is the Joule heating and D_i is the ID of the microchannel.

The inner wall temperature $T_{\text{w,in}}$ can be solved though the one-dimensional heat conduction equation in cylindrical coordinates:

$$T_{\text{w,in}} = T_{\text{w,out}} - \frac{\ln\left(\frac{D_o}{D_i}\right) q D_i}{2k}, \quad (3)$$

where $T_{\text{w,out}}$ represents the temperature on the inner side of the ITO/Ag deposition layer and is considered equal to the outer wall temperature that can be measured by the thermocouple, D_o is the OD of the microchannel and k is the heat conductivity of the microchannel.

The measured pressure loss can be separated into components as

$$\Delta P_{\text{total}} = \Delta P_{\text{sub}} + \Delta P_{\text{sat}}, \quad (4)$$

where ΔP_{sub} and ΔP_{sat} are the pressure losses in the sub-cooled liquid region and saturated boiling region, respectively. ΔP_{sub} can be calculated by iteration of the following equations (Eqs. (5)–(7)). First, l is arbitrarily assumed for calculating ΔP_{sub} :

$$\Delta P_{\text{sub}} = f \frac{1}{2} \rho U^2 \frac{l}{D_i}, \quad (5)$$

where f is the friction factor for laminar Poiseuille flow, ρ the liquid density and U is the bulk mean velocity. The saturation pressure P_{sat} at $x = l$ is given by

$$P_{\text{sat}}(l) = P_{\text{in}} - \Delta P_{\text{sub}}, \quad (6)$$

where P_{in} is the inlet pressure. Then, the saturation temperature T_{sat} is calculated from the saturation table of the refrigerant [11]. Finally, the new value of l is obtained from the energy balance as

$$\int_0^l q(x) \pi D_i dx = \dot{M} C_p (T_{\text{sat}}(l) - T_{\text{in}}). \quad (7)$$

The iterative calculation using Eqs. (5)–(7) is repeated until the value of l converges.

The local pressure distribution $P_{\text{sat}}(x)$ in the saturated boiling region is assumed to be linearly distributed along the tube, and given by

$$P_{\text{sat}}(x) = P_{\text{sat}}(l) - \Delta P_{\text{sat}} \frac{x-l}{s}, \quad (8)$$

Finally, h is calculated as

$$h = \frac{q}{T_{w,\text{in}} - T_{\text{ref}}}, \quad (9)$$

where T_{ref} is the local bulk mean temperature. When the fluid is in the saturated region, T_{ref} is equal to T_{sat} , and is derived from P_{sat} [11].

4. Definition of average local heat transfer coefficient h

Defining the steady state in microchannels is extremely difficult due to large fluctuations in pressure and temperature time history [3,4]. However, with the aid of a high-speed camera, Yen et al. [12] reported that the flow field shows semi-periodic variation in the flow patterns. Therefore, in our study, when the deviation of such semi-periodic variation dropped below $\pm 5\%$, measurement of the wall temperature and pressure loss was started. For both the circular and square microchannels, it took about 20–30 min to reach this semi-periodic variation. To obtain a more accurate averaged data, temperature and pressure measurement data for h were obtained within a 1-hour time period.

Using the same technique used by Yen et al. [7], propagation of uncertainties in the data reduction error in the data reduction method described above [13] was estimated here using ANSI/ASME PTC 19.1. According to the estimation of the accuracy in the test sections and in the measurement devices propagated through data reduction

procedure, the final uncertainty in h could be controlled within $\pm 10\%$ in all experimental data if the wall superheat exceeded 2.5°C . Therefore, only the data in which the wall superheat exceeded 2.5°C were taken as reliable experimental data in this study.

5. Experimental results

5.1. Heat transfer characteristics for different shaped cross-sections at the same heat flux q , mass flux \dot{m} and inlet pressure P_{in}

According to the work by Steiner and Taborek [14], convective boiling in conventional tubes can be divided into two mechanisms: nucleate boiling dominance and convective boiling dominance. In conventional tubes, when $\chi < 0.5$, the nucleate boiling effect dominates and the convective boiling effect diminishes, whereas when $\chi > 0.5$, the convective boiling effect becomes dominant and the nucleate boiling effect diminishes.

Fig. 6 shows h versus χ under the same q , \dot{m} and P_{in} ($P_{\text{in}} = 163 \text{ kPa}$) but different shaped microchannels. In both the circular and square microchannels, h decreased with increasing χ , similar to all previous experimental results for microchannels [2,3,7]. At $\chi < 0.4$, h in the square microchannel was much larger than that in the circular microchannel, whereas when $\chi > 0.4$, h was similar for both the square and circular microchannels. The flow visualization revealed that bubble nucleation only occurred when $\chi < 0.4$. Therefore, $\chi = 0.4$ is considered to be the critical χ for nucleate and convective boiling dominance in microchannels. These results for the heat transfer characteristics in these microchannels indicate that the shape of the cross-section significantly affects the bubble nucleation mechanism but has relatively little effect on the convective boiling mechanism.

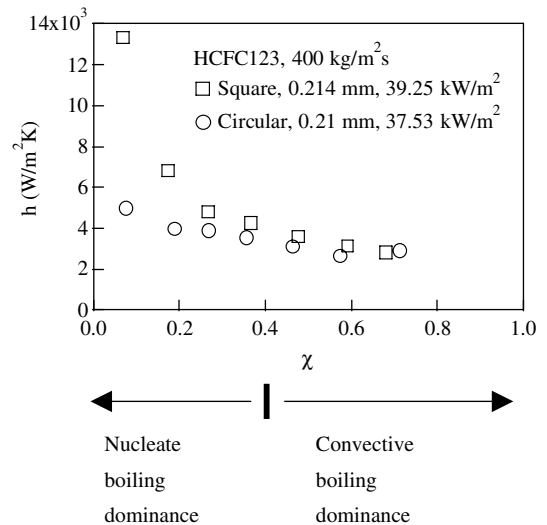


Fig. 6. Local heat transfer coefficient h versus vapor quality χ for different shaped cross-sections at the same q and \dot{m} .

5.2. Heat transfer characteristics in the nucleate boiling dominance region in microchannels with different shaped cross-sections

Figs. 7 and 8 show the observed flow patterns in the square and circular cross-sections of the microchannels at $\chi \sim 0.07$. In both the square and circular cross-sections at the same observation point, flow patterns showed periodic variation as described in the preceding section, including bubbly, plug, annular and capillary flow patterns. A capillary flow pattern represents independent droplets moving along the inner wall of the test section (e.g., [15]).

According to Hetsroni et al. [4], the reason for such large flow pattern variations is the extremely limited space in the microchannels, in which the bubbles grow in both the downstream and upstream direction simultaneously and thus push the working fluid into other channels, thus leading to radical flow pattern variation. However, our results (Figs. 7 and 8) show that similar flow pattern variation and reverse flow still occurred in the single microchannel experiments. Because the experimental loop included 1-mm-ID stainless steel tubes and 0.25-mm-ID Teflon tubes (Fig. 1), the damping of the experimental sys-

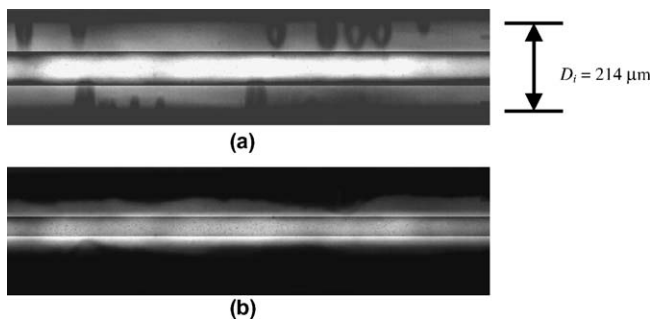


Fig. 7. Flow patterns visualized in a 0.214-mm-ID square microchannel at $\dot{m} = 400 \text{ kg/m}^2\text{s}$, $q = 39.25 \text{ kW/m}^2$ and $\chi = 0.069$. (a) Bubbly flow and (b) annular flow.

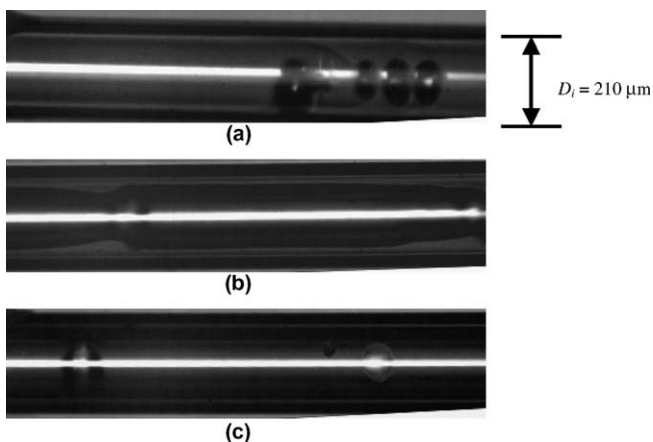


Fig. 8. Flow patterns visualized in a 0.21-mm-ID circular microchannel at $\dot{m} = 400 \text{ kg/m}^2\text{s}$, $q = 37.53 \text{ kW/m}^2$ and $\chi = 0.074$. (a) Bubbly flow, (b) annular flow and (c) capillary flow.

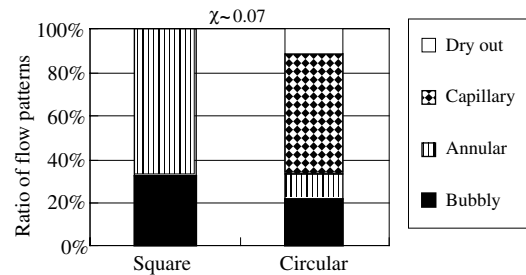


Fig. 9. Ratios of flow patterns in a period under different cross sections at the same low vapor quality in the same experimental run of Fig. 6. $\chi \sim 0.07$, $h = 13336 \text{ W/m}^2\text{K}$ for square microchannel and $h = 5003 \text{ W/m}^2\text{K}$ for a circular microchannel.

tem was considered very small. Therefore, the pressure fluctuation generated from bubble nucleation must have been large to lead to reverse flow, and the main reason for the flow pattern variation might be the large pressure fluctuations generated from bubble nucleation rather than interaction between parallel microchannels. The period of flow pattern variation varied from 0.08 to 0.12 s, depending on q . Because the onset of bubble nucleation requires large pressure fluctuations, bubble nucleation at low \dot{m} and q becomes very difficult. Finally, severe liquid superheat phenomena always occur at low \dot{m} and q [7].

Fig. 9 shows the percentage of each type of flow pattern region in a representative period of flow pattern variation at relatively low χ under the same q , \dot{m} and P_{in} but different shaped cross-sections in the same experimental run shown for Fig. 6. At low χ (~ 0.07), the period of the flow pattern variation in the square cross-section ($\tau = 0.1071 \text{ s}$) was larger than that in the circular cross-section ($\tau = 0.0841 \text{ s}$). A large region of capillary flow pattern (55.1%) within a period was observed in the circular microchannel. In contrast, the region of bubbly flow pattern in the square microchannel (33.11%) was about 10% larger than that in the circular microchannel (22.48%) because square microchannels have a higher number of active nucleation sites and nucleation bubbles due to the corners acting as active nucleation sites (see Figs. 7 and 8). The parallel lines in the center of Figs. 7 and 8 are the results of adjustment of brightness in the center region of the pictures because of high reflectivity in the center region. These experimental observations correspond to the bubble nucleation model by Li and Cheng [16], who investigated the bubble nucleation model by Hsu [17] and expanded the model to include nucleation from corners in microchannels. According to the model by Li and Cheng, corners in microchannels can effectively trap the initial gas nuclei and lower the nucleation temperature of the working fluid. On the other hand, since the bubbly flow pattern still exists in circular microchannel, the experimental result might reflect the compound effects of the shape and the surface roughness in microchannels. The effect of surface roughness usually depends on different surface materials (see [18]). In this paper, by applying the same material (Pyrex glass) to the two test sections with different cross-sections, the effect of different material should be

minor. The experimental results of bubble nucleation under different surface materials can be found in [18].

Compared to the circular microchannel, the constitution of flow patterns in the square microchannel was simpler. In the square microchannel, only bubbly flow and annular flow patterns were typically observed, and capillary flow pattern was rarely observed. Moreover, the complete dry-out region, which is considered to drastically reduce h , was not observed in the square microchannel.

Fig. 10 shows an illustration of the liquid film evaporation process based on our observations using the high-speed camera. In the square microchannel, dry-out of the liquid film always started at the center of the inner wall in an annular flow pattern. As evaporation proceeded, the contact line retreated to corners and formation of moving independent droplets became difficult. In contrast, in the circular microchannel, the liquid film was distributed evenly on the inner wall. As evaporation proceeded, the thickness of the liquid film decreased evenly, thus providing a good environment for the formation of independent droplets. Fujita et al. [19] carried out flow visualization experiments of pool boiling and measured the boiling curve in narrow gaps (5, 2, 0.6, and 0.15 mm). In their experiments, a partial dry-out region was seldom observed when the gap was larger than 0.6 mm. In contrast, when the gap was 0.15 mm, nucleation bubbles tended to expand in the horizontal direction with partial dry-out along the inner walls. Our convective visualization results for the circular microchannel coincide with these observations because a large percentage (55.1%) of capillary flow pattern was observed. In a square microchannel, corners stabilize the liquid film as reported by Wayner [20], who observed micro layer evaporation in micro heat pipes. Such stability prevents complete dry-out, which occurred in the circular microchannel (Fig. 9) and resulted in decreased h .

Moriyama and Inoue [21] measured the liquid film thickness in a narrow gap (0.1–0.4 mm in width) and established an empirical correlation between liquid film thickness and the width of the gap. By combining this empirical correlation and our experimental results from

our current study, a model of film evaporation can be established in future theoretical work.

Based on all of the above-mentioned current and previous observations, the two main reasons for high h in a square microchannel at $\chi < 0.4$ are that (1) corners act as effective nucleation cavities and (2) no dry-out and capillary flow regions appear due to a relatively stable evaporation process. In contrast, annular flow patterns in both the square and circular microchannels have similar heat transfer characteristics, as discussed next.

5.3. Heat transfer characteristics in the convective boiling dominance region in different shaped cross-sections

At high χ (>0.4), no bubble nucleation was observed by the high-speed camera, indicating convective boiling dominance. As shown in Fig. 6, local h in the convective boiling dominance region was similar for both the square and circular microchannels. Fig. 11 shows the percentage of flow pattern regions in a representative period of flow variation at higher χ in the same experimental run shown in Fig. 6. At higher χ , the flow patterns consisted only of annular flow and dry-out regions. Moreover, the flow patterns were similar for both the circular and square microchannels. The similarity in both the local h and constitution of flow patterns indicates that annular flow patterns have similar heat transfer characteristics in both square and circular microchannels.

5.4. Comparison of heat transfer characteristics for different shaped cross-sections and mini tubes

Tran et al. [22] measured h of convective boiling in a brass mini tube (2.46 mm ID) and a brass mini rectangular channel (2.4 mm width). Different from our experimental results for circular and square microchannels, their experimental results show very little difference in h between the circular and square minichannels.

Based on the comparison between experimental results of minichannel by Tran et al. and microchannels in this study, the shape of the cross-sections is crucial for the heat transfer characteristics in microchannels because the number of active nucleation sites is relatively smaller in

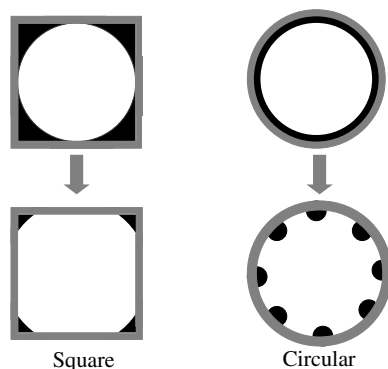


Fig. 10. Illustration of liquid film evaporation process for square and circular cross-sections of microchannels based on visualization observations.

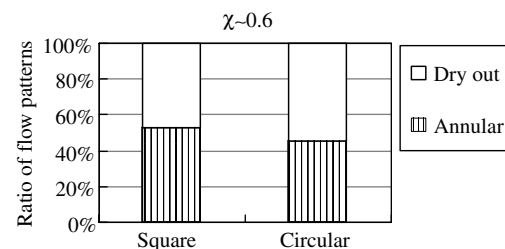


Fig. 11. Ratios of flow patterns in a period under different cross-sections at the same high vapor quality in the same experimental run as in Fig. 10. $\chi \sim 0.6$, $h = 3135 \text{ W/m}^2\text{K}$ for a square microchannel and $h = 2664 \text{ W/m}^2\text{K}$ for a circular microchannel.

microchannels compared with the number in minichannels. Therefore, the corners in microchannels, which have thicker liquid film for higher temperature gradient and can serve as active nucleation sites, become a dominant factor in h when $\chi < 0.4$. In contrast, in larger ID channels (2.4 mm), the effect of the cross-section shape diminishes due to relatively larger number of cavities distributed along the inner wall of the channel. Compared to cavities on the plane of the inner wall of a square minichannel, the corners have relatively little importance as active nucleation sites.

5.5. Effect of heat flux q and mass flux \dot{m} on heat transfer characteristics for different shaped cross-sections

Fig. 12 shows h for different q in a square microchannel at medium \dot{m} (400 kg/m²s). At the nucleate boiling dominant region ($\chi < 0.4$), higher q led to higher h . These results contradict experimental results for SUS 304 circular microtubes reported by Yen et al. [7], in which h was reportedly independent of q . Fig. 13 shows h for different q in the circular microchannel at the same \dot{m} (400 kg/m²s). Different from the square microchannel, h was apparently independent of q , as reported by Yen et al.

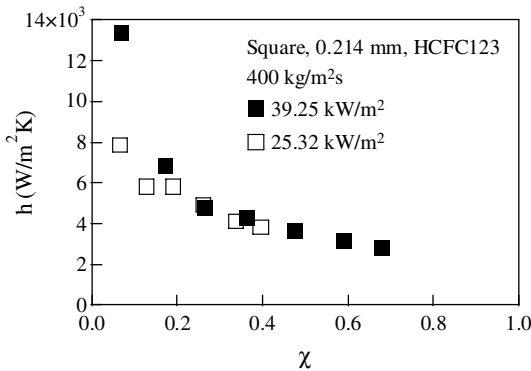


Fig. 12. Local heat transfer coefficient h versus vapor quality χ for different heat flux q in a 0.214-mm-ID square microchannel at medium mass flux \dot{m} .

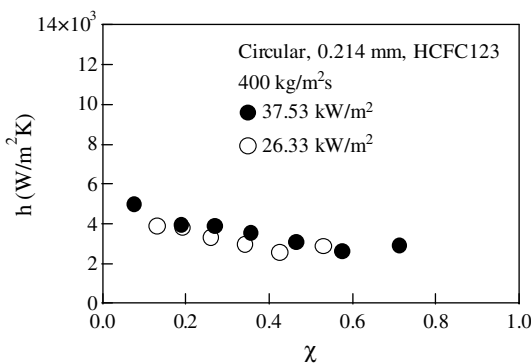


Fig. 13. Local heat transfer coefficients versus vapor quality under different heat fluxes in 0.21 mm circular microchannel, medium mass flux.

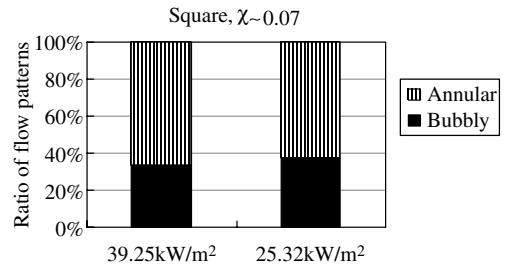


Fig. 14. Ratios of flow patterns in a period under different cross sections at two different heat fluxes in the same experimental run of Fig. 12. $\chi \sim 0.07$, $h = 13336$ W/m²K for $q = 39.25$ kW/m² and $h = 7837$ W/m²K for $q = 25.32$ kW/m².

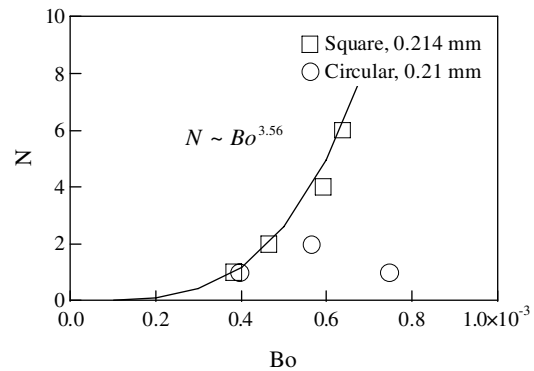


Fig. 15. Number of nucleation sites N versus boiling number Bo for square and circular cross-sections of microchannels.

Fig. 14 shows the percentage of flow pattern regions in a representative period of flow variation in the same experimental run of Fig. 12 under different q at low χ (~ 0.067). Although h was higher at this higher q , the constitution of the flow patterns was similar for both the high and low q . In contrast, flow visualization revealed that the number of active nucleation sites was much higher for higher q in the square microchannel. It is also much higher in the square microchannel than in the circular microchannel. Fig. 15 shows the number of active nucleation cavities N versus boiling number Bo in all experimental runs. In the square microchannel, N increased with increasing Bo :

$$N \sim Bo^{3.56}, \tag{10}$$

where boiling number can be defined as follows:

$$Bo = q/h_{lv}\dot{m}. \tag{11}$$

h_{lv} is the latent heat of the working fluid.

The relationship between N and Bo coincides with the experimental results reported by Griffith and Wallis [23], in which the x -axis was wall superheat and y -axis was nucleation density. According to Griffith and Wallis, the power n in Eq. (10) depends on the type of working fluid, and this dependence is on the same order as in Eq. (10). This similarity in the relationship between N and Bo implies that corners in square microchannels have similar bubble nucleation characteristics to active cavities in pool boiling.

In contrast, in the circular microchannel, N was independent of Bo , and only 1 or 2 nucleation sites existed along the test section. The independence of N on Bo indicates independence of h from q and \dot{m} in circular microchannels.

Moreover, in the circular microchannel, the active nucleation sites only existed at certain larger cavities regardless of q and \dot{m} , whereas in the square microchannel nucleation sites differed in location depending on the different q and \dot{m} . The very limited number of nucleation sites in the circular microchannel led to insufficient bubble nucleation at low χ ,

resulting in low h when $\chi < 0.4$. Different from the circular microchannel, the square microchannel had unlimited possible nucleation sites due to the existence of corners. Corners can enrich the working liquid, leading to thicker liquid film, so that bubble nucleation continues to occur from the corner even in plug and annular flow patterns due to larger temperature gradient of the thicker film in the corners, as shown in Fig. 16.

In conclusion, q apparently strongly affects the number of nucleation sites in square microchannels when $\chi < 0.4$. Corners in square microchannels can serve as effective

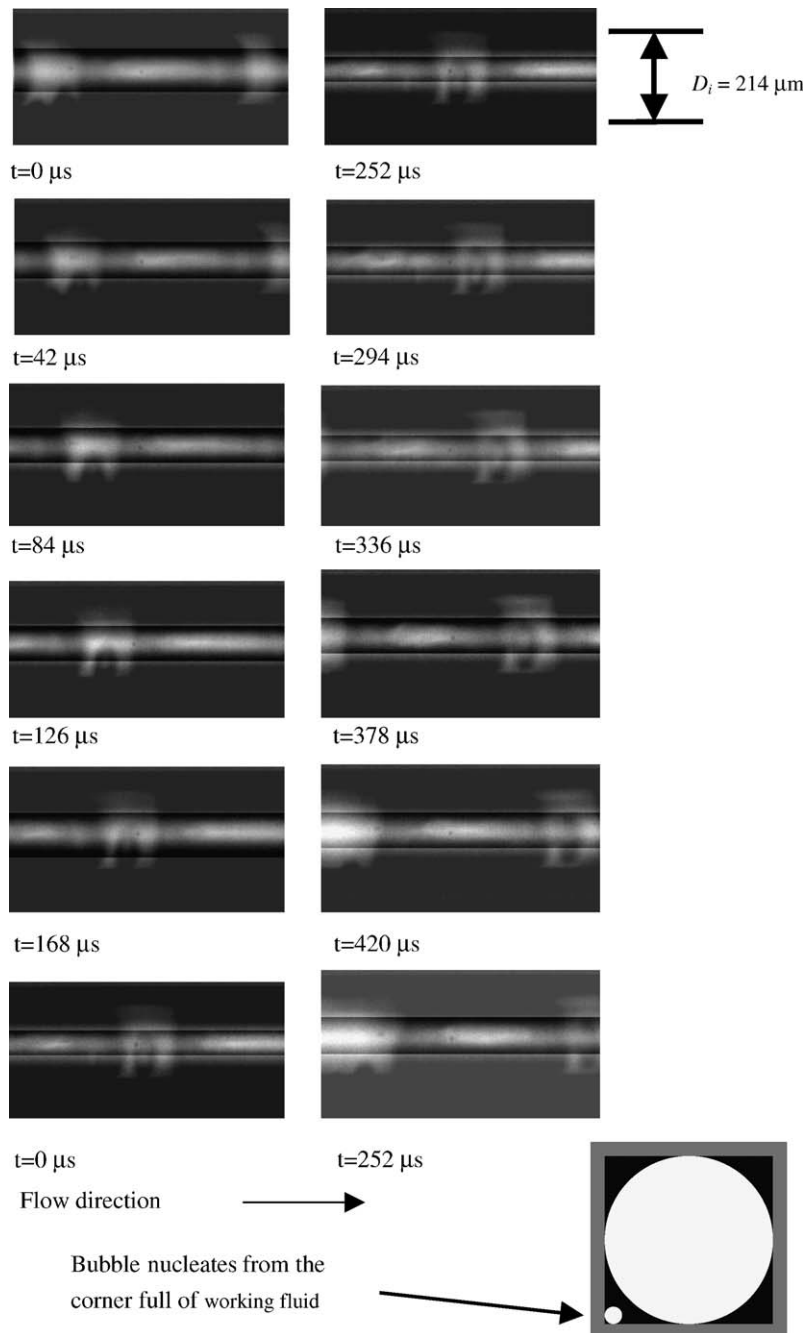


Fig. 16. Above: Bubble nucleation from the corner in plug flow pattern in a 0.214-mm-ID square microchannel. Below: Illustration of bubble nucleation in plug flow pattern.

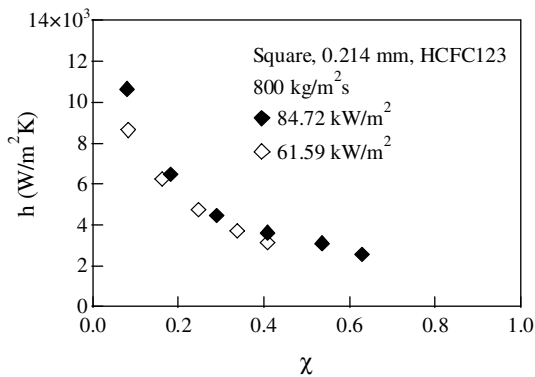


Fig. 17. Effect of heat flux q on local heat transfer coefficient h versus vapor quality χ in a 0.214-mm-ID square microchannel at high heat flux q and mass flux \dot{m} .

nucleation sites, the number of which is highly related with local heat transfer coefficient. In circular microchannels, however, if the inner wall is smooth, there would be no cavities for bubble nucleation and h would then be mainly affected by annular and slug flow patterns and become independent of χ , as shown in the experimental results for smooth titanium microtubes reported by Yen et al. [24].

Fig. 17 shows h versus χ in the square microchannel at higher q and \dot{m} . Although h increased with increasing q in the square microchannel (Fig. 12), h became independent of q and \dot{m} when $q > 40 \text{ kW/m}^2$, $\dot{m} > 800 \text{ kg/m}^2\text{s}$. This independence is similar to the experimental result for the circular microchannel (e.g., Yen et al. [24]). The reason for such limitation of h is due to the confined space in the microchannel, which limits bubble growth. Fig. 18

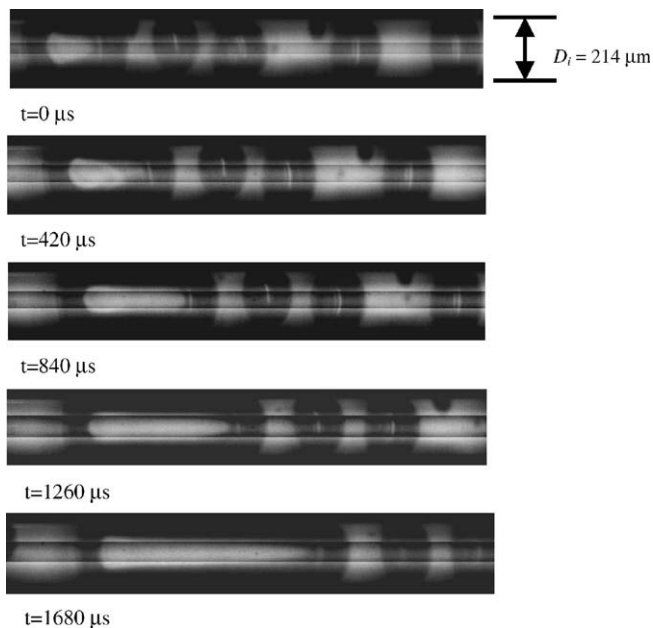


Fig. 18. Limited bubble growth in a 0.214-mm-ID square microchannel. Mass flux $\dot{m} = 400 \text{ kg/m}^2\text{s}$, heat flux $q = 39.25 \text{ kW/m}^2$, vapor quality $\chi = 0.11$.

shows high-speed camera images of bubble expansion in the square microchannel at $\dot{m} = 400 \text{ kg/m}^2\text{s}$ and $q = 39.25 \text{ kW/m}^2$. Only one of the several nucleation bubbles in the images had room to expand. Such limitation of bubble growth explains the limitation of h .

Based on the above observation (Figs. 17 and 18), the concept of critical Bo being responsible for the independence of h on q and \dot{m} can be established. The critical Bo was about 6.0×10^{-4} in the square microchannel and less than 4.0×10^{-4} in the circular microchannel, and was apparently related to ID and to the shape of the cross-section of the microchannel. Below the critical Bo , h depended on q . However, when Bo exceeded the critical Bo , h was independent of q and \dot{m} .

6. Comparison of experimental results to empirical correlations

Comparing to the recent number of experimental results on microchannels, reports on empirical correlations and heat transfer models are relatively few. Here, currently accepted empirical correlations and heat transfer models in microchannels are discussed and verified with the experimental results from this study.

Kandlikar [8] proposed an empirical correlation for convective boiling in microchannels:

$$h = 0.6683Co^{-0.2}(1-x)^{0.8}h_{\text{single}} + 1058.0Bo^{0.7}(1-x)^{0.8}F_{\text{FI}}h_{\text{single}}, \quad (12)$$

where Co is the convection number representing the effect of χ and its relevant flow pattern and has the following form:

$$Co = \left(\frac{1-\chi}{\chi}\right)^{0.8} \left(\frac{\rho_v}{\rho_l}\right)^{0.5}, \quad (13)$$

where h_{single} is the single phase heat transfer coefficient and F_{FI} is a fluid-dependent parameter.

Eq. (12) is the modified form of the empirical correlation for conventional tubes [25]. Fig. 19 compares the experimental data from our study and the empirical correlation

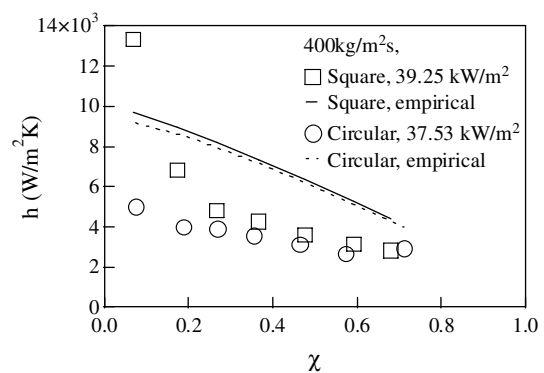


Fig. 19. Comparison between current experimental results and empirical correlations by Kandlikar [8].

in Eq. (12) by Kandlikar [8]. The empirical correlation predicts fairly well the h for the square microchannel, but not for the circular microchannel, especially in the low χ region (<0.4). Comparison between this empirical correlation and the conventional empirical correlation [25] reveals that the major contributor to this empirical correlation is the nucleate boiling term (90% of the value in the empirical correlation is from the nucleation boiling term). Such a high contribution indicates the dominance of nucleate boiling in square microchannels and indicates the insufficiency in predicting experimental results of circular microchannels, in which bubble nucleation becomes relatively minor.

The empirical correlation expressed in Eq. (12) predicts fairly well the results in square microchannels, which are the commonly used cross-section in industrial applications. For theoretical interest and higher accuracy for circular microchannels, however, a heat transfer model that corresponds better to the visualization results is needed. Recently, models based on the time history of flow pattern variation observed from experiments for single microchannels and parallel microchannels have been proposed by Thome et al. [26], Yen et al. [27] and Hetsroni et al. [28]. Advanced effort into correctly predicting the heat transfer characteristics of bubble nucleation and each flow pattern in microchannels becomes crucial for improving the accuracy of these time-dependent models.

7. Conclusions

Visualization experiments with simultaneous measurement of the local heat transfer coefficient in microchannels with different shaped cross-sections were carried out. Semi-periodic variations in the flow patterns were observed, and such variations led to large pressure fluctuations.

The heat transfer coefficient was higher for the square microchannel because corners in the square microchannel acted as effective active nucleation sites. In contrast, lack of cavities in the smooth glass circular microchannel yielded a relatively smaller heat transfer coefficient at lower vapor quality.

In the square microchannels, the heat transfer coefficient became independent of heat flux when the critical boiling number exceeded a critical value. This independence is due to the confined space that limits the bubble growth.

A previously reported empirical correlation reported by Kandlikar [8] focusing on nucleate boiling mechanism roughly predicted our experimental results in the square microchannel. In contrast, a time-dependent model that better reflects the actual flow patterns is needed for predicting the local heat transfer coefficient in circular microchannels.

Acknowledgements

The authors thank Prof. Kato at the University of Tokyo and Mr. Sasaki at Elionix for their help in obtaining the SEM photos.

References

- [1] S. Paitoonsurikarn, N. Kasagi, Y. Suzuki, Optimal design of micro bare-tube heat exchanger, in: Symposium Energy Engineering in the 21st Century, Hong Kong, China, 2000, pp. 972–979.
- [2] T.S. Ravigururajan, Impact of channel geometry on two-phase flow heat transfer characteristics of refrigerants in microchannel heat exchangers, *Trans. ASME: J. Heat Transfer* 120 (1998) 485–491.
- [3] M.E. Steinke, S.G. Kandlikar, Flow boiling and pressure drop in parallel microchannels, in: First International Conference on Microchannels and Minichannels, April 24–25, 2003.
- [4] G. Hetsroni, A. Mosyak, Z. Segal, E. Pogrebnyak, Two-phase flow patterns in parallel microchannels, *Int. J. Multiphase Flow* 29 (2003) 341–360.
- [5] H.Y. Wu, P. Cheng, Visualization and measurement of periodic boiling in silicon microchannels, *Int. J. Heat Mass Transfer* 46 (2003) 2603–2614.
- [6] S. Saitoh, H. Daiguji, E. Hihara, Boiling heat transfer and pressure drop of HFC134a in horizontal small-diameter tubes, in: Proceedings of the 39th National Heat Transfer Symposium of Japan, Sapporo, Japan, 2000, pp. 667–668.
- [7] T.-H. Yen, N. Kasagi, Y. Suzuki, Forced convective boiling heat transfer in microtubes at low mass and heat fluxes, *Int. J. Multiphase Flow* 29 (2003) 1771–1792.
- [8] S.G. Kandlikar, Heat transfer mechanisms during flow boiling in microchannels, *Trans. ASME: J. Heat Transfer* 126 (2004) 9–16.
- [9] P.-C. Lee, F.-G. Tseng, C. Pan, Bubble dynamics in microchannels. Part I: single microchannel, *Int. J. Heat Mass Transfer* 47 (25) (2004) 5575–5589.
- [10] P.M.-Y. Chung, M. Kawaji, The Effect of channel diameter on adiabatic two-phase flow characteristics in microchannels, *Int. J. Multiphase Flow* 30 (2004) 735–761.
- [11] REFPROP, Thermodynamic and transport properties of refrigerants and refrigerant mixtures, NIST standard reference database 23 (1998) version 6.01.
- [12] T.H. Yen, Y. Suzuki, N. Kasagi, Visualization of convective boiling in a micro tube with simultaneous measurement of local heat transfer, in: Proceedings of the 1st International Forum Heat Transfer, November, 2004, Kyoto, pp. 119–120.
- [13] ANSI/ASME, An American national standard, part 1 measurement uncertainty. PTC 19.1, 1985.
- [14] D. Steiner, J. Taborek, Flow boiling heat transfer in vertical tubes correlated by an asymptotic model, *Heat Transfer Eng.* 13 (1992) 43–69.
- [15] V.P. Carey, *Liquid–Vapor Phase-Change Phenomena*, Hemisphere Publishing Corporation, 1992.
- [16] J. Li, P. Cheng, Bubble cavitation in a microchannel, *Int. J. Heat Mass Transfer* 47 (12) (2004) 2689–2698.
- [17] Y.Y. Hsu, On the size range of active nucleation cavities on a heating surface, *Trans. ASME: J. Heat Transfer* 84 (1962) 207–216.
- [18] T.H. Yen, Heat transfer characteristics of forced convective boiling in a micro tube at low heat and mass fluxes, Ph.D. dissertation, The University of Tokyo, 2004.
- [19] Y. Fujita, H. Ohta, S. Uchida, K. Nishikawa, Nucleate boiling heat transfer and critical heat flux in narrow space between rectangular surfaces, *Int. J. Heat Mass Transfer* 31 (2) (1988) 229–239.
- [20] P.C. Wayner, Intermolecular forces in phase-change heat transfer: Kern award review, *AIChE J.* 45 (10) (1998) 2055–2068.
- [21] K. Moriyama, A. Inoue, Thickness of the liquid film formed by growing bubble in a narrow gap between two horizontal plates, *ASME: J. Heat Transfer* 118 (1996) 133–139.
- [22] T.N. Tran, M.W. Wambsganss, D.M. France, Small circular- and rectangular-channel boiling with two refrigerants, *Int. J. Multiphase Flow* 22 (1996) 485–498.
- [23] P. Griffith, J.D. Wallis, The role of surface conditions in nucleate boiling, *Chem. Eng. Prog. Symp. Ser.* 56 (49) (1960) 49.

- [24] T.-H. Yen, Y. Suzuki, N. Kasagi, Effects of fluid properties and system pressure on convective boiling in microtubes, in: Proceedings of the 1st International Symposium on Micro and Nano Technology, March, Honolulu, Hawaii (CD-ROM), 2004, Paper VII-1-03.
- [25] S.G. Kandlikar, A general correlation for saturated two-phase flow boiling heat transfer inside horizontal and vertical tubes, *Trans ASME: J. Heat Transfer* 112 (1990) 219–228.
- [26] J.R. Thome, V. Dupont, A.M. Jacobi, Heat transfer model for evaporation in microchannels. Part I: presentation of the model, *Int. J. Heat Mass Transfer* 47 (14) (2004) 2891–3589.
- [27] T.-H. Yen, Y. Suzuki, N. Kasagi, Modeling on convective boiling heat transfer in a micro tube based on flow visualization, in: Proceedings of the 6th World Conference Experimental Heat Transfer, Fluid Mechanics and Thermodynamics, April 17–21, Matsu-shima, Japan (CD-ROM), 2005, Paper 4-a-9.
- [28] G. Hetsroni, A. Mosyak, E. Pogrebnyak, Z. Segal, Explosive boiling of water in parallel microchannels, *Int. J. Multiphase Flow* 31 (2005) 371–392.